Prod. Eng. Res. Devel. (2016) 10:253–263
DOI 10.1007/s11740-016-0674-7

COMPUTER AIDED ENGINEERING

Computation of thermo-elastic deformations on machine tools a study of numerical methods

Andreas Naumann[4] · Norman Lang[2] · Marian Partzsch[1] · Michael Beitelschmidt[1] · Peter Benner[2,3] · Axel Voigt[4] · Jörg Wensch[4]

Received: 20 October 2015 / Accepted: 20 April 2016 / Published online: 29 April 2016
© German Academic Society for Production Engineering (WGP) 2016

Abstract Modern machine tools are highly optimized with respect to their design and the production processes they are capable to. Now for further advances, especially a detailed knowledge about the thermo-elastic behavior is needed, because the nowadays still existing deficits are mainly related to this. That is why, endeavors in improvement, like the optimization of the design, the evaluation of new materials and the regulation of the production process, particularly rely on accurate computed thermal deformations. One possible approach to increase their quality is to also include the relevant structural variabilities of the machine tools as well as the resulting interactions between the coupled parts within the calculations. In this article, three different numerical methods are presented, which include structural motions in thermo-elastic analyses. Thereby, several conflicting criteria, like real-time capability, memory saving issues and accuracy are fulfilled each time in a different manner. Those methods are afterwards compared with respect to their runtime and accuracy. Finally, the paper concludes with a classification of the usability of the methods in real-time control and optimization tasks.

✉ Andreas Naumann
andreas.naumann@tu-dresden.de

[1] Institute for Solid Mechanics, Technische Universität Dresden, Dresden, Germany

[2] Faculty of Mathematics, Technische Universität Chemnitz, Chemnitz, Germany

[3] Max Planck Institute for Dynamics of Complex Technical Systems, Magdeburg, Germany

[4] Institute for Scientific Computing, Technische Universität Dresden, Dresden, Germany

Keywords Thermo-elasticity · Structural variability · Finite element analysis · Long time integration · Model order reduction

1 Introduction

Modern machine tools are high precision production systems. Several heat sources create a time-varying inhomogeneous temperature field resulting in a structural deformation of the machine. With that, a problematic, thermally caused displacement of the Tool Center Point (TCP) is induced, directly causing unwanted manufacturing defects for the work piece. Considering all possible error sources for the performance of machine tools, nowadays, approximately 50–80 % of the overall defects are thermally driven, see e.g., [13]. Countering these defects in an energy efficient way, for instance via design optimizations or an active in-process correction of the thermal TCP-displacement are focal points of the CRC/TR 96.[1] The development and application of improvement approaches like these will inevitably be based on thermal analyses, emphasizing their relevance in the progress of modern machine tool engineering.

In general, a proper modelling of the thermo-elastic behavior of an entire machine tool requires a profound knowledge of the heat flow between their single components [11]. Furthermore, the motion of the TCP is mechanically realized by components of the frame structure which move relative to each other. That is why modeling the thermo-elastic behavior requires to take the structural

[1] Collaborative Research Center/Transregio 96—"Thermo-Energetic Design of Machine Tools," http://transregio96.de.

variability into account. Now in this paper, three different numerical approaches for the thermo-elastic analysis, which also consider the structural variability of the components, are presented. These methods are described in detail by means of an exemplary stand-headstock-system (a part of a milling machine, see Fig. 1), which was also considered in [6] within a thermal analysis using compact models.

In Sect. 2, a short introduction to the exemplary system, including the relevant thermal and dislocation boundary conditions, is presented. Then, the first approach which incorporates structural variability within the proprietary FE-software ANSYS (Sect. 3) is described. Its main purpose is to provide detailed results gained within a reliable software environment to serve as a reference for verification. The second approach considers a realization in the open-source FE software AMDiS, combining adaptive mesh refinement and a time integration scheme based on *Defect Corrected Averaging* (DCA), see Sects. 4 and 6, respectively. This method enables the inclusion of advanced numerical modelling and integration methods within the analysis, so that a detailed computation of extensive long term problems becomes possible, too. Next, Sect. 5 considers a model order reduction (MOR) wherein the structural variability is considered via a parametric dependency of the reduced system. With this approach, a real-time computability of a few selected thermal deformations of the machine tool is achieved which may subsequently be used for an active control of the production process. Finally, several comparisons of these approaches are presented in Sect. 7.

2 Thermo-elastic problem with structural variability

The subsequently introduced numerical methods have been developed for the particular usage within the development and operation of machine tools, especially to calculate their thermal dependend displacements while considering relevant structural variabilities. So for the comparison of their performances, we are interested in such a motion-containing problem, which furthermore is related to the specific field of machine tool engineering. That is why we chose the system of a headstock relatively moving to its stand (see Fig. 1/left) as the subject of interest in our methodological studies. Here we want to emphasize, that we are only interested in using the later presented, potential numerical representation of such a system which contains all the specific features our different numerical methods need to be able to deal with. If the model itself is actually able to map the reality appropriatly or not is basically irrelevant for our question. Despite of that, we want to mention that the given model in conjunction with the progress of the single boundary conditions (see Fig. 1) has been aligned with the results of a physical experiment done at the *Institute of Machine Tools and Control Engineering* at *Technische Universität Dresden* (see [6]). In particular, the following features are considered within the used numerical model in general, each carried out in the additionally stated way:

- The heat conduction within each structural component is governed by Fourier's law. The standard values of steel are used, hence heat conduction $\lambda = 50\ \frac{\mathrm{W}}{\mathrm{mK}}$, heat capacity $c = 460\ \frac{\mathrm{J}}{\mathrm{kgK}}$, and density $\rho = 7200\ \frac{\mathrm{kg}}{\mathrm{m}^3}$.
- The heat exchange between system and environment is modelled by convective boundary conditions $\dot{q}_R = \alpha(T_R - T_{sys})$, with an ambient temperature T_R, the temperature of the system T_{sys} and a convective exchange coefficient α. The affected surfaces can be seen in the left table of Fig. 1 with their related values of air, ground and oil exchange coefficents, respectively, and hourly updated ambient temperatures in the table at the right of Fig. 1. The color-gradiented heads of the table indicate that, due to its motion, the ambient temperature of headstock is chosen either in the top or middle layer of the air.
- A motion of the headstock along the grey depicted guidance rail (see Fig. 1/left). The actual considered motion profiles for the specific simulations are presented below.
- The friction caused by the motion is considered via a heat flux input on the contact zone. We use a hydrostatic thin film friction model $\dot{q}_{fric} = \beta|v|^2$ that solely depends on the velocity $|v|$ and an assumed friction coefficient $\beta = 9.9\ \frac{\mathrm{kWs}^2}{\mathrm{m}^4}$. The frictional heat is distributed equally between the headstock and stand.
- The involved bodies are thermally coupled due to a heat conduction through the contact. It is evaluated as a heat flux $\dot{q}_{ex} = \alpha_C(T_{stand} - T_{stock})$ using the present temperatures T_{stand} and T_{stock} in the contact zone of the stand and the stock, respectively, and a thermal contact conductance coefficient $\alpha_C = 50\ \frac{\mathrm{W}}{\mathrm{m}^2\mathrm{K}}$.
- The thermal dependent displacements are calculated in static structural analyses. Therefore we also use the standard material values for steel, i.e Young's modulus $E = 210 \cdot 10^9\ \frac{\mathrm{N}}{\mathrm{m}^2}$, Poisson's ration $\nu = 0.3$ and thermal expansion coefficient $\alpha_\epsilon = 12 \cdot 10^{-6}\ \frac{1}{\mathrm{K}}$.
- The stand is fixed to the ground, i.e. we apply a zero-displacement boundary condition at the ground surface of the stand.
- At the remaining surfaces, we assume zero forces, i.e. Neumann boundary conditions for the displacement equations.

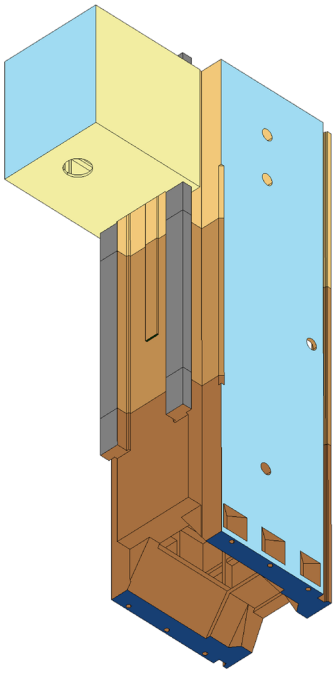

Hour	$\alpha = 10\,\mathrm{W/m^2K}$			$\alpha = 100\,\mathrm{W/m^2K}$	
	Top	Middle	Bottom	Oil	Ground
01	23,41°C	23,08°C	22,67°C	22°C	20°C
02	21,72°C	21,70°C	21,25°C		
03	22,23°C	21,80°C	21,74°C		
04	23,40°C	22,94°C	22,45°C		
05	23,76°C	23,42°C	23,11°C		
06	24,50°C	24,12°C	24,07°C		
07	24,88°C	24,50°C	24,36°C		
08	24,69°C	24,49°C	24,22°C		
09	23,94°C	23,61°C	23,13°C		
10	23,05°C	22,96°C	22,48°C		
11	22,43°C	22,08°C	22,00°C		
12	22,07°C	22,05°C	21,57°C		
13	21,83°C	21,69°C	21,21°C		
14	21,45°C	21,43°C	21,18°C		
15	21,65°C	21,60°C	21,20°C		
16	21,53°C	21,12°C	21,05°C		
17	21,19°C	20,84°C	20,63°C		

Fig. 1 The *left* part shows the different areas for the boundary conditions of the stand and the headstock. *Each color* corresponds to an ambient temperature. The *grey* parts depict the rail, those surfaces which are affected by the combined motion dependen friction and exchange loads. In the *right* part, the temperatures and exchange coefficients for each hour and boundary area are listed

To describe a general working day, the room temperatures increase in the first 6 h and decrease towards the end time. Our production process consists of different movement speeds in the three different areas "lower half", "upper half" and "complete rail". Within 3 h, we fixed the velocities, but changed the movement areas. This leads to the different period lengths, which are described in Table 1. Because of the piecewise constant velocities, the movement is periodic in time. Because of the increasing velocity, the period lengths decrease. This leads to higher frictional heat sources towards the end of the simulated time. However, the frictional heat flux increases due to the quadratic dependence on velocity. Therefore, we expected to see the different production phases in the temperature profile.

In the course of a numerical analysis of the given transient, thermo-elastic problem with the temperature vector $\mathbf{T}$ and the displacement vector $\mathbf{u}$ as its field variables and $\dot{\mathbf{q}}$ and $\mathbf{F}$ as the related thermal and structural load vectors, the spatially discretization yields the following ODE system

$$\begin{bmatrix} 0 & 0 \\ 0 & M^{el} \end{bmatrix} \begin{pmatrix} \ddot{\mathbf{T}} \\ \ddot{\mathbf{u}} \end{pmatrix} + \begin{bmatrix} C^{th} & C^{elth} \\ 0 & C^{el} \end{bmatrix} \begin{pmatrix} \dot{\mathbf{T}} \\ \dot{\mathbf{u}} \end{pmatrix} + \begin{bmatrix} D^{th} & 0 \\ D^{thel} & D^{el} \end{bmatrix} \begin{pmatrix} \mathbf{T} \\ \mathbf{u} \end{pmatrix} = \begin{pmatrix} \dot{\mathbf{q}} \\ \mathbf{F} \end{pmatrix}. \tag{1}$$

In this ODE system, the matrices C^{th}, C^{el}, D^{th}, D^{el} and M^{el} represent the thermal and elastic capacity matrix, the thermal and elastic stiffness matrix and the mass matrix of the elastic part, respectively. Furthermore, the coupling effects, represented via $C^{elth}\dot{\mathbf{u}}$ (piezo-caloric effect) and $D^{thel}\mathbf{T}$ (thermal expansion), cause nonsymmetric system matrices. It can be seen that the piezo-caloric effect, which

Table 1 Velocities v and corresponding period lengths ϵ at different time intervals, where each interval lasts one hour, i.e. the first time slot begins at t = 1 h and ends at t = 2 h

t (h)	v (m/min)	ϵ (s)	t (h)	v (m/min)	ϵ (s)	t (h)	v (m/min)	ϵ (s)
[1,2)	2.5	12	[4,5)	5	6	[7,8)	10	3
[2,3)	2.5	48	[5,6)	5	24	[8,9)	10	12
[3,4)	2.5	12	[6,7)	5	6	[9,10)	10	3
[10,11)	15	2	[13,14)	20	1.5			
[11,12)	15	8	[14,15)	20	6			
[12,13)	15	2	[15,16)	20	1.5			

causes the increase of temperature due to an impact of the structural field, depends on the first time derivative of the deformations, hence the strain rate and not the resulting strains itself. Now the only deformations that will occur in our analysis are the thermally dependent ones, which reasonably can be expected to evolve relatively slow and homogenous, because of the comparatively inert character of the thermal field itself. That is why it is a valid assumption to neglect any transient structural behavior $\dot{\mathbf{u}} = \ddot{\mathbf{u}} = \mathbf{0}$ and thus the piezo-caloric effect. With this and in conjunction with using the method of weak coupling in which the field interactions are considered in the load vectors, the involved field problems are decoupled. We obtain the system

$$\begin{aligned} C^{th}\dot{\mathbf{T}} + D^{th}\mathbf{T} &= \dot{\mathbf{q}} \\ D^{el}\mathbf{u} &= \mathbf{F} - D^{thel}\mathbf{T}\,, \end{aligned} \tag{2}$$

which represents the non-iterative thermo-elastic analysis.

Next to its various benificial impacts on the required calculation effort, this approach also requires to consider the structural motions solely within the thermal part of the analysis. Within the following sections, we describe in detail how the moving components are realized in the different used FE-packages and simulation approaches.

3 Using contact-technology in proprietary FE-software

A motion-containing, thermo-elastic analysis within the proprietary software-package ANSYS has been developed, mainly to provide reliable results that can be used in verifying the mathematically more sophisticated methods introduced in the subsequent sections.

Now within a transient, thermal analysis, a motion is included by the approach of stepwise adjusting the position of the moving body (illustrated black to purple in Fig. 2/left). ANSYS enables this way of considering structural variability by providing a contact-technological class of element types. In our particular case, we use a pair of *Target-/Contact-Elements* for identifying the position of the moving part with respect to the stationary one (Pinball-Algorithm, circles in Fig. 2/left) and for including their interaction ($\dot{q}_{ex}$) in the analysis between each other.

Due to a non-existing normal force, the frictional heat flux $\dot{q}_{fric}$ cannot be calculated directly and therefore has to be predetermined like an ordinary, time dependent load. At last, moving and stationary bodies are NEUMANN-loaded with the sum of the evaluated load parts as seen in Fig. 2/left and afterwards treated as separate thermal FE-problems. Applying this, leads to a quite intuitive and simple method for modeling FE-problems containing translational motions.

Now, the actual process chain of modeling and meshing primarily follows geometric and load-related requirements of the thermally analyzed problem. Including translational motions affects this chain merely to a slight extent. The only thing to do is to use the *Sweep-Method* when meshing regions near the moving contact – in our example: the rail and guidance regions. This leads to a uniform mesh in the direction of motion. Therefore, the basic, CAD-imported solid is separated within ANSYS Workbench at a favorable location, so that parallel free and mapped meshing of the resulting parts is possible. It is recommended to use a *Bonded-Contact* with infinite conductance for combining the different meshes. Its defining constraints are automatically included in the system equations and therefore inexpensive during the following analysis. At the contact-surfaces of the motion, a numerically robust *No-Separation-Contact* is applied, as there is no need to take structural motion out of the contact plane into account in a pure thermal analysis.

When solving the system, in mathematical terms the stepwise motion represents an abrupt change in loading for the stationary body leading to major miscalculations when using a generalized trapezoidal rule with explicit contributions for ODE-integration. Therefore, it is essential to evaluate the 1st-order system gained by a spatial discretized thermal field with the implicit EULER-method to find a solution.

The solution process is mainly done as usual, starting with an initial time-step and the definition of position-

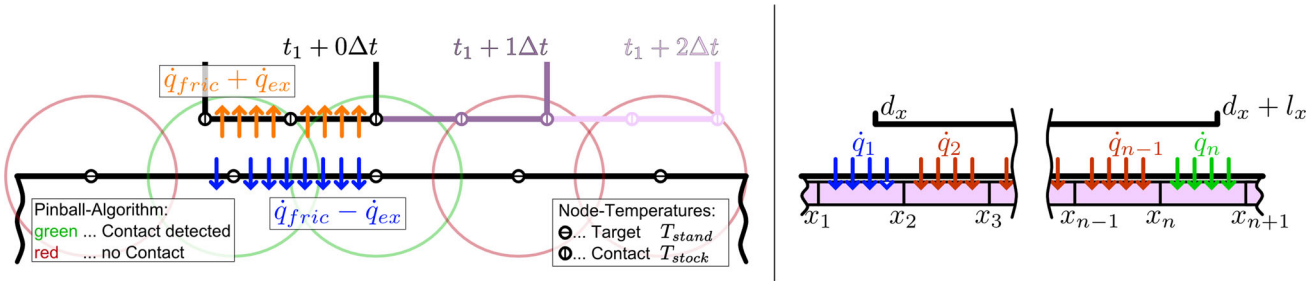

Fig. 2 *Left* structural variability with contact-technology. *Right* frictional heat flux on stationary body—from [14]

independent loads. This also includes the position itself, which is defined by a predetermined time-dependent displacement (DIRICHLET boundary condition) applied to all structural DOFs (rigid-body motion) in their respective coordinate direction.

As stated above, $\dot{q}_{fric}$ requires a manual application. Assuming a motion parallel to the x-axis, the location of heat input at the stationary body varies discretely with time, but can be uniquely described by the present displacement d_x of the moving body and its length l_x. In general, one obtains a model structure as depicted in Fig. 2/right with partially covered element layers on the edges of the contact area. As we can see, it is important to adjust the value of the applied heat flux for these layers to ensure the correct amount of heat input. The heat fluxes for the element layers in contact (with partial or total coverage) are followed by linear interpolation to:

$$\dot{\mathbf{q}}_1 = \frac{x_2 - d_x}{x_2 - x_1}\dot{q}_{fric}, \quad \dot{\mathbf{q}}_n = \frac{d_x + l_x - x_n}{x_{n+1} - x_n}\dot{q}_{fric}$$
$$\text{and} \quad \dot{\mathbf{q}}_{2,\ldots,n-1} = \dot{q}_{fric}$$

As one can see, the necessity of this edge-layer NEUMANN-load scaling is independent of the time step size and, therefore, only negligible, if an extremely fine spatial discretization is applied.

4 Realization in open-source FE-software

The essential problem in FE-analysis of coupled problems is the coupling of different meshes, representing the coupled geometries. In our case, this coupling arises from the exchange boundary conditions. Due to high memory and runtime requirements of the proprietary software ANSYS, we implemented the model problem in the open-source FE-toolbox AMDiS.[2] In this section, we explain the modelling of the mesh coupling in open-source FE-software. Because of the static nature of the elastic part, we concentrate on the evolution of the temperature field in the remaining section.

The open-source FE-software AMDiS allows more flexibility to incorporate the moving components. Two independent meshes are considered for both components, the stand and the headstock. They are adaptively refined towards the rail and the motion of the headstock is again modeled as a rigid body motion by changing the coordinates of the mesh and described by the function $X(t, x)$.

The aforementioned problem of partially covered element layers at the contact zone is here circumvented by extending the contact zone to the whole rail using

$$\chi_2(t,x) = \begin{cases} 1, & x \in \text{contactzone}, \\ 0, & \text{else}. \end{cases}$$

The fluxes due to exchange at the rail can now be written as

$$\dot{q}_{ex,stock} = \chi_2(t, X(t,x))\alpha_C(T_{stand} - T_{stock})$$
$$\dot{q}_{ex,stand} = \chi_2(t, X(t,x))\alpha_C(T_{stock} - T_{stand})$$

and provide the coupling of the heat conduction problem in the headstock and the stand. We use linear finite elements for the discretization, which is realized in AMDiS [18]. Together with the linear elasticity problem, the resulting system reads as Eq. (2), however now with a modified heat flux term $\dot{\mathbf{q}}$ and a time-varying thermal diffusion matrix D^{th}, which for the thermal part reads

$$\underbrace{\begin{bmatrix} C_1^{th} & 0 \\ 0 & C_2^{th} \end{bmatrix}}_{C^{th}} \underbrace{\begin{bmatrix} \dot{\mathbf{T}}_1 \\ \dot{\mathbf{T}}_2 \end{bmatrix}}_{\dot{\mathbf{T}}} = \underbrace{\begin{bmatrix} D_1^{th}(t) & B_{12}(t) \\ B_{21}(t) & D_2^{th}(t) \end{bmatrix}}_{D^{th}(t)} \underbrace{\begin{bmatrix} \mathbf{T}_1 \\ \mathbf{T}_2 \end{bmatrix}}_{\mathbf{T}} + \underbrace{\begin{bmatrix} B_1 & 0 \\ 0 & B_2 \end{bmatrix} \begin{bmatrix} \mathbf{z}_1(t) \\ \mathbf{z}_2(t) \end{bmatrix}}_{\dot{\mathbf{q}}} \tag{3}$$

with 1, 2 corresponding to stand and headstock respectively. Analogous to the thermal problem in Eq. 2, we have the capacity matrices C_j^{th}, the diffusion matrices D_j^{th} and the two coupling matrices B_{21} and B_{12} for each component $j = 1, 2$. Furthermore, the heat flux $\dot{\mathbf{q}}$ consists of the two fluxes $B_1\mathbf{z}_1(t)$ and $B_2\mathbf{z}_2(t)$, where the $\mathbf{z}_j(t)$ contain the corresponding environment temperatures from the boundary conditions and the matrices B_1 and B_2 stem from the finite element discretization. The thermo-mechanical contact problem was solved with mortar finite elements, in [10]. The ODE (3) has to be solved, with a suitable numerical solver [16] over an operative time, which corresponds to the timescale of the temperature conduction. The described movement, with a periodicity in the range of a few seconds requires time integrators that are attached to the smallest timescale. Due to the mesh resolution, the matrix $D^{th}(t)$ has negative and in magnitude large eigenvalues. Therefore, explicit methods are constrained by very small timesteps. and we have to use an implicit method. We choose the second-order time linear implicit integrator ROS2, see [17]. Implicit methods need the solution of linear equation systems in every timestep. Within linear implicit methods, the same matrix is used several times, which reduces the number of LU-decompositions. Furthermore this time integrator belongs to the class of W-methods, hence we can reuse the matrix during several timesteps.

In Sect. 6, we will discuss a further improvement of the time integration, taking a possible periodicity of the mapped motions into account.

[2] AMDiS - **A**daptive **M**ulti-**Di**mensional **S**imulations, www.amdis-fem.org/.

5 Model order reduction for thermo-elastic systems

In order to improve storage and computational demands of the high-resolution FE model, describing the thermo-elastic behaviour of the machine structure, in this section we aim at finding a surrogate model to (2) that has a significantly lower dimension. Therefore, a certain model order reduction technique is to be applied such that a low-dimensional model retaining the system structure and appropriately approximating the original system is obtained.

Here, we only consider one of the differential algebraic subsystems (2) describing the thermo-elastic behavior of the stand or the headstock geometry, respectively, since both equations have the same mathematical structure. As described in Sect. 1, the structural variability induced by the moving headstock has to be modeled in an appropriate way. In the remaining part of this section, let the external forces be considered as $F = 0$, as given in the example in Sect. 7. Since the movement of the headstock actually yields a time dependent model of the form (2), here we consider the linear time-varying (LTV) thermo-elastic model

$$\begin{aligned} C^{th}\dot{\mathbf{T}}(t) &= D^{th}(t)\mathbf{T}(t) + B(t)\mathbf{z}(t), \\ D^{el}\mathbf{u}(t) &= -D^{thel}\mathbf{T}(t), \\ \mathbf{y} &= G\mathbf{u}(t), \end{aligned} \tag{4}$$

where

$$\begin{aligned} &C^{th} := C_j^{th} \in \mathbb{R}^{n_{th}\times n_{th}}, D^{th}(t) := D_j^{th}(t) \in \mathbb{R}^{n_{th}\times n_{th}}, \\ &B(t) := \left[\tilde{B}_j(t), \quad B_j\right] \in \mathbb{R}^{n_{th}\times m} \text{and } \mathbf{z} := \begin{bmatrix} \mathbf{T}_\mathrm{i} \\ \mathbf{z_j} \end{bmatrix} \in \mathbb{R}^{\mathrm{m}} \end{aligned} \tag{5}$$

with $i, j = 1, 2,\ i \neq j$. Here, $\tilde{B}_j(t) \in \mathbb{R}^{n_{th}}$ represents the active contact region of the guide rails of the stand, and the remaining matrices and inputs $\mathbf{z_j}$ are as given in Equations (2) and (3). Further, $\mathbf{y}$ denotes the displacement outputs (e.g., observations of the TCP displacement). That is, $G \in \mathbb{R}^{p\times n_{el}}$ maps the deformation field $\mathbf{u}$ to the observed outputs $\mathbf{y}$. Moreover, n_{th} denotes the number of thermal FE degrees of freedom (DOFs), $n_{el} = 3n_{th}$ the number of elastic DOFs, m the number of inputs and p the number of outputs of the system. Given the one-sided coupling of the thermo-elastic model, using the Schur complement, i.e., inserting the elasticity equation into the output, as described in [5], the special differential algebraic structure of (4) is exploited. Therefore, we obtain the model equation

$$\begin{aligned} C^{th}\dot{\mathbf{T}}(t) &= D^{th}(t)\mathbf{T}(t) + B(t)\mathbf{z}(t), \\ \mathbf{y} &= \tilde{G}\mathbf{T}(t) \end{aligned} \tag{6}$$

of dimension n_{th} instead of $n = n_{th} + n_{el} = 4n_{th}$ with the modified output matrix $\tilde{G} := -G(D^{el})^{-1}D^{thel}$ including the entire information of the elastic model. Note, that we can assume the invertibility of the matrix D^{el} because of the fixing boundary conditions at the ground.

Note that we uncouple the thermo-elastic subsystems of the stand and the headstock by considering the average temperature $\bar{\mathbf{T}}_i$ at the contact area of the subsystem i to be an input to the subsystem j. Therefore, the coupling matrices B_{ij} in Sect. 4 are replaced by the auxiliary matrices $\tilde{B}_j(t)$ representing the contact area of subsystem j. Thus, the uncoupling allows us to apply the chosen MOR procedure to the respective subsystems independently.

As mentioned above, in order to reduce the computational time and the storage needed to save the system data, e.g. for real-time use on a micro controller, the main goal now is to apply model order reduction to the system (6). For a comprehensive overview on model reduction see, e.g., [1]. Model order reduction aims at computing a reduced-order model (ROM) of the form

$$\begin{aligned} C_r^{th}\dot{\mathbf{T}}_r &= D_r^{th}(t)\mathbf{T_r} + B_r(t)\mathbf{z}, \\ \mathbf{y_r} &= G_r\mathbf{T_r}, \end{aligned} \tag{7}$$

such that, using the same input signal $\mathbf{z}$ as for the original model (6), the reduced-order output $\mathbf{y_r}$ satisfies $\mathbf{y_r} \approx \mathbf{y}$. That means, the ROM captures the system behavior of the full order model (FOM) (6).

Using a projection based MOR technique, we need to find truncation matrices $V, W \in \mathbb{R}^{n\times r}$ such that the reduced-order matrices are computed in the form

$$\begin{aligned} &C_r^{th} = W^T C^{th} V,\ D_r^{th}(t) = W^T D^{th}(t) V \in \mathbb{R}^{r\times r}, \\ &B_r(t) = W^T B(t) \in \mathbb{R}^{r\times m},\ G_r = \tilde{G}V \in \mathbb{R}^{p\times r} \end{aligned} \tag{8}$$

with $r \ll n$. Here, the superscript $(.)^T$ denotes the transposing of the quantity $(.)$.

In [12, Section 4], system (6) is considered to be parameter dependent. Therein, the time-dependence of (6) is mapped to a parameter $\mu = \mu(t)$ describing the moving position of the headstock at the guide rails of the machine stand. Thus, we define the parametric system

$$\begin{aligned} C^{th}\dot{\mathbf{T}} &= D^{th}(\mu)\mathbf{T} + B(\mu)\mathbf{z}, \\ \mathbf{y} &= \tilde{G}\mathbf{T}. \end{aligned} \tag{9}$$

Following the ideas presented in [2], as a first step towards finding global truncation matrices V, W, feasible for all admissible values μ, we choose k parameter sample points $\mu_\ell, \ell = 1, \ldots, k$. Now, using the iterative rational Krylov algorithm (IRKA) [8], we compute pairs $V_\ell, W_\ell \in \mathbb{R}^{n\times r_\ell}$ for each fixed sample point μ_ℓ. Finally, these local projection matrices are concatenated to the global reduction bases

$$V = [V_1, \ldots, V_k], \quad W = [W_1, \ldots, W_k]$$

of dimension $n \times r$ with $r = \sum_{\ell=1}^{k} r_\ell$.

In order to avoid the computation of the reduced-order matrices $D_r^{th}(\mu), B_r(\mu)$ for each stand-headstock configuration associated to μ, as in (8), we setup a parameter affine representation of the parameter dependent matrices in the form

$$\begin{aligned} D^{th}(\mu) &= D_0^{th} + f_1(\mu)D_1^{th} + \cdots + f_{m_A}(\mu)D_{m_D}^{th}, \\ B(\mu) &= B_0 + g_1(\mu)B_1 + \cdots + g_{m_B}(\mu)B_{m_B}, \end{aligned} \tag{10}$$

where $m_D, m_B \in \mathbb{N}$. Note, that the numbers of summands m_D and m_B do not necessarily have to be equal. Further, it is always possible to achieve such a parameter affine representation, see e.g., [9]. An artificially generated affine representation for the example presented here is also explained in [12, Section 4]. Given the affine form, the parameter dependent matrices $D^{th}(\mu), B(\mu)$ can be reduced to the form

$$\begin{aligned} \hat{D}^{th}(\mu) &= \sum_i^{m_A} f_i(\mu) W^T D_i^{th} V, \\ \hat{B}(\mu) &= \sum_i^{m_B} g_i(\mu) W^T B_i, \end{aligned} \tag{11}$$

where the computation of $W^T D_i^{th} V$ and W_i^{TB} is parameter independent and therefore performed only once in advance of the actual parameter study.

The forward simulation based on the ROM is performed with the implicit EULER-scheme, as for the ANSYS computations, see Sect. 3.

6 Defect-corrected-averaging for coupled systems

The coupled thermo-elastic problem consists of a fixed stand and a moving headstock, as described in Sect. 2. In case of a periodic velocity profile, the movement is also periodic and uniform. Furthermore, the velocities are large, which in turn leads to small period lengths. The classic methods, used in Sect. 4, are constrained by this small timescale. On the other hand, we are interested in the thermo-elastic evolution over several hours, which corresponds to the timescale of conduction. In the remaining section, we concentrate on the thermal part and neglect the elastic equations.

Both timescales together renders the ODE (3) in a multiscale problem. An introduction to the solution of multiscale problems using the "heterogenous multiscale" approach can be found in [4]. We will use the "defect corrected averaging" method [7], which is an extension of the "stroboscopic averaging" from [3], It is an asynchronous multirate method and consists of two phases:

- Initialization phase:
  - Compute the time average $\overline{D}^{th}$ of the diffusion matrix $D^{th}(t)$.
  - Solve the oscillatory thermal problem (3) from t_0 to $t_0 + \epsilon$ with a small micro timestep $h_m \ll \epsilon$.
  - Use the solution of the previous step and the average diffusion matrix $\overline{D}^{th}$ and compute a constant auxilliary source $\dot{\mathbf{q}}_c$, which leads to the same solution as the oscillatory problem. This is accomplished with the iterative linear solve GMRES [15] together with an appropriate preconditioner.
- Solution phase: Solution of the linear ODE $\dot{\mathbf{T}} = \overline{D}^{th}\mathbf{T} + \dot{\mathbf{q}}_c$ with constant coefficients utilizing large macro timesteps $H \gg \epsilon$.

The first step involves the solution of the oscillatory thermal problem over one period ϵ. This is done with the two stage W-method ROS2, described in [17]. For the solution phase, we have chosen the same time integrator, but much larger timesteps.

The long time problem includes several speeds and moving areas of the headstock, as can be seen in Table 1. They lead to 15 oscillatory sources. Therefore, we have to repeat the initialization phase 15 times, i.e., once with every combination of moving area and velocity.

7 Comparison of solutions

In this section, we compare the simulated temperatures and displacements, which were computed with the three methods described in the Sects. 3–6. The open source FE-toolbox AMDiS and the commercial FE-software ANSYS computet temperature profiles on the full geometry. For the MOR method, we selected 6 reference points, shown in Fig. 3.

Due to the large memory and runtime requirements for the contact formulation in ANSYS, we have selected a shorter time interval of only 1 hour for the comparison of all methods. To compare the solutions of AMDiS and ANSYS in space, we selected the black line on the rail, as shown in the right part of Fig. 3.

Only the FE-simulation using the open-source FE-toolbox AMDiS and the model order reduction approach were used to compute the temperature and dislocation fields over the entire time interval of 0–16.5 h.

7.1 Short time comparison

The short time comparison tests consist of parts from the long time tests. We used the timespan $t = [5-6]h$ with the corresponding velocity from Table 1 and room temperature from the table in Fig. 1.

The solution with the commercial FE-software ANSYS was done with a mixed mesh with hexagons near the

coupling boundary and tetrahedra in the remaining parts. This mesh consists of 31 653 cells in total and 72 452 nodes including the quadratic nodes. Here, we selected the implicit EULER-scheme with a stepsize of 1.0 second.

The solution with the FE-program AMDiS is obtained with the same mesh as for the long time simulation having 16,626 nodes and 49,482 tetrahedra. Our time integrator is the second-order ROS2 method with a time step of 0.6 seconds, which corresponds to 40 steps in one period. This model also serves as the basis for the MOR procedure, described in Sect. 5. Using the MOR method, a ROM of dimension $r = 75$ was generated. The chosen reduced order dimension r is due to a desired relative error of order 10^{-3}. That is, the dimension was determined by a number of numerical computations such that a relative error of about one per thousand compared to the full order model could be reached. The reduction process took around $1h$. Still, this is performed only once in advance of the actual simulation and, therefore, does not affect the timings of the computation of the temperature and displacement field. For the simulation we used an implicit EULER-scheme with timesteps of the size $\delta t = 10s$. Note that the rather high oscillatory movement of the headstock within the $10s$ is treated by an additional averaging of the inputs z_j. Here, the average over 1000 samples within the timestep of $10s$ is taken. We compare the solutions in six points over the entire time interval. The temperature evolution in the points 1-3, and 4-6, is presented in Fig. 4 (left) and (right), respectively. As the figures show, the solutions are very close to each other. Additionally, we compare the temperature profiles of both FE-simulations after 1 h in Fig. 5. Again, both solutions are close to each other.

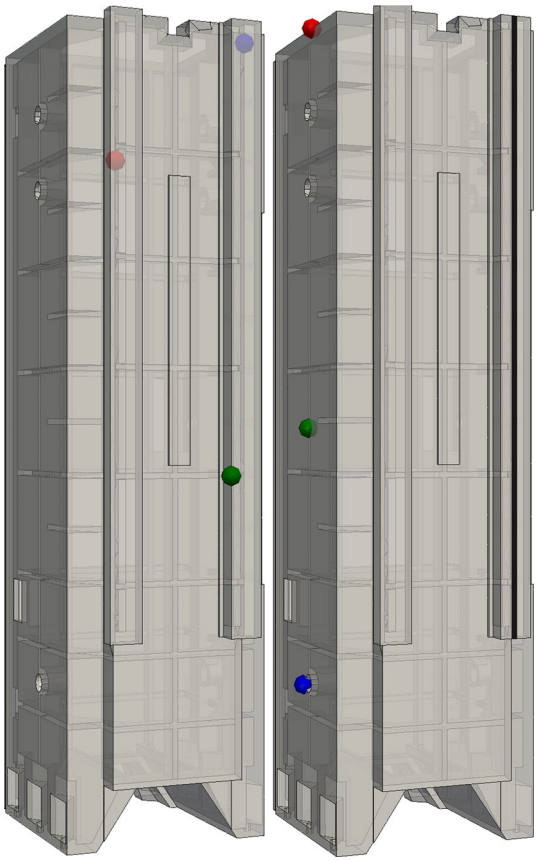

Fig. 3 Machine stand with reference points 1–6. The *left* figure shows the reference points 1–3 in the *colors red*, *green* and *blue*, respectively, whereas the *right* figure shows the reference points 4–6 in the *colors red, green* and *blue*, respectively (color figure online)

7.2 Long time comparison

The long term study was only feasible using the open-source FE-software AMDiS and the MOR approach. We will compare the different time integrations utilized in the FE-approach, denoted by ROS2 and DCA, see Sects. 4 and 6, respectively. As described in Sect. 2, we have a time increasing heat source. Therefore, we expect to see the different production phases in the six reference points, which are shown in the Fig. 3. The three points in the left of Fig. 3 reside on the rail and are mainly effected by the frictional heat. The other three points, seen on the right of

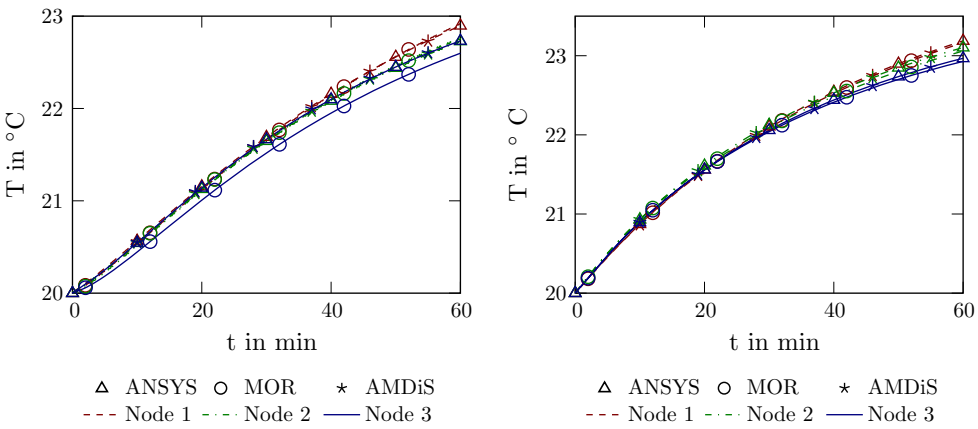

Fig. 4 Comparison of the temperature evolution in points 1–3 (*left*) and 4–6 (*right*)

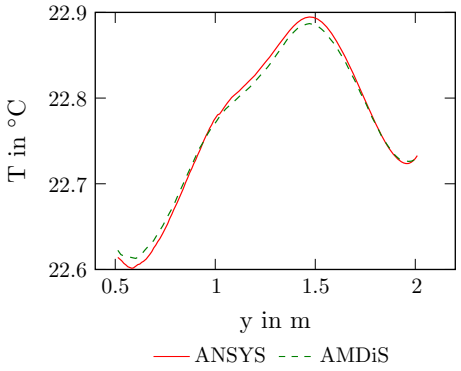

Fig. 5 Comparison of the temperatures on the path (*black vertical line* from *bottom* to *top*, i.e. $y = 0$ is located at the ground) at the right rail in Fig. 3

Fig. 3, lie on the convective boundary and follow the ambient temperature.

The computation of the temperature profiles were done with the following method parameters:

- In the FE-approach, the W-method, described in Sect. 4, was run using the second-order ROS2 as the time integrator. To account for the different timescales, we selected two different timesteps. In the pure conduction phase, i.e., hour 0–1 and hour 16–16.5, we used large timesteps $\delta t = 3$ min. In the oscillatory phases, a period constrained timestep of $\delta t = \epsilon/30$ was chosen. The complete simulation took 4 days on a desktop machine with two cores at 3 GHz. This simulation serves as a reference solution for the other approaches.
- The simulation setup for the MOR approach for the long term comparison coincides with the short term scenario. That is, the ROM with $r = 75$ and the implicit EULER time integrator with a time step of 10.0 seconds for the forward simulation were used. This corresponds to approximately $\frac{1}{5}$ to 6 oscillations, which can be seen in Table 1. The simulation of the entire time horizon of 16.5 h based on the ROM took around $2s$. These results were executed on a 64 bit CentOS 5.5 system with two Intel® Xeon® X5650@2.67 GHz with a total of 12 cores and 48 GB main memory without using parallel programming.
- The FE-approach with the defect corrected averaging scheme was run with a stepsize H = 30 seconds for the solution phase. During the initialization phase, we took the micro scale step size $h_m = \epsilon/80$. The complete thermal simulation took 1.5 h on a desktop machine with one core at 3 GHz.

A direct comparison of the computational times are also given in Table 2. The corresponding temperature and deformation fields at the observed points 1–6 are shown in Fig. 6. Points 1–3 are located at the rail (see Fig. 3), which

Table 2 System dimensions and corresponding computational times of the ROS2/DCA, and the MOR approach

	AMDiS		MOR
	ROS2	DCA	
System order	16,626	16,626	80
Reduction time	–	–	1 h
Simulation time	4 days	1.5 h	2 s

means they are most influenced by the frictional heat flux. Even in those points, the first 8 h are mainly determined by the room temperatures. With the beginning of the 8th hour, the temperatures increase fast above the ambient temperature. Especially the green curve in Fig. 6 (left) shows, which part, i.e. the frictional heat source or the ROBIN boundary condition, of the model has which influence at which time. For example, in the time range of hour 10–13, the temperature increases first sharply, because the headstock moves in the center area. Thus the green point is most influenced by the friction. In the next hour, the movement affects the entire rail, so the effective heat inflow next to the green point decreases. But the ambient temperature near the rail remains active and the heat flows out with time. In hour 12–13, the movement is restricted to the upper part, which, in turn, leads to a sharper temperature decrease in this hour. The different time integrations used in the FE-simulations and the MOR results agree well in these points. The same agreement is also shown for the three points on the right, they are located away from the rail and are therefore less critical. For the deformation fields, we only consider the FE-simulation with DCA and obtain again a good agreement. All differences between the considered approaches are below 10 %, which confirms the applicability of the considered approximations with respect to time integration using DCA and with respect to the model reduction using the ROM. Moreover, we like to state that the ROS2 and the DCA approach are indispensable for an accurate model validation and in order to possibly support the modeling process itself by delivering valuable information of model inaccuracies. Given a validated model, and when a significant number of model simulation repetitions or, even more important, the applicability of the thermo-elastic model to a machine controller enter the spotlight, the necessity of a reduced order model becomes obvious, as the computation times reveal, see Table 2.

8 Summary

In this paper, we have presented different numerical approaches for analyzing thermo-elastic behavior of machine tools. All approaches have two essential qualities:

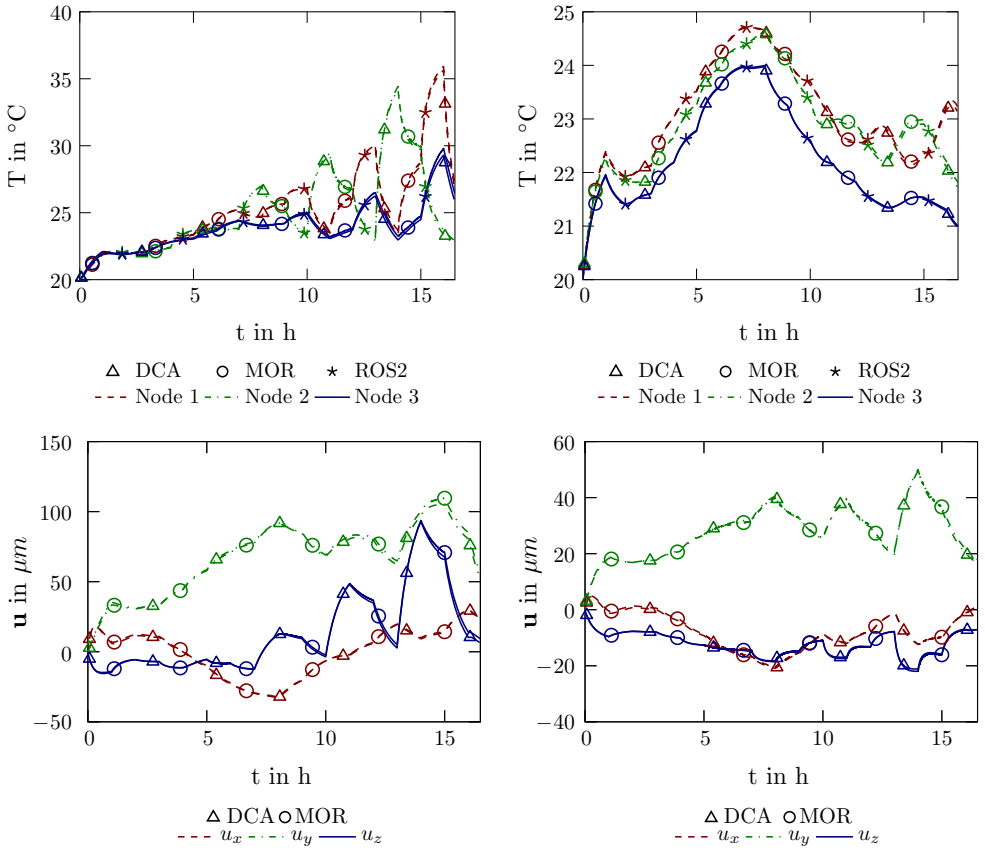

Fig. 6 Comparison of the temperature (*top*) and deformation (*bottom*) in points 1–3 (*left*) and 4–6 (*right*)

1. enabling a module-based modeling of the coupled parts
2. considering the structural variabilities of the system

The results in Sect. 7 show that all of the presented approaches yield basically the same results. The errors between the methods lie in a single-digit percent range. However, the approaches significantly differ in the required computing time.

The ANSYS approach with a simple EULER time discretization requires the largest computational effort. The approach was not feasible for the considered long time simulation over 16 h. The second approach used the linear implicit time integrator ROS2, which allowed to solve the long time problem but still only within an inacceptable time. However, the solution serves as a reference solution for further approximations. This approach was implemented in the open-source FE toolbox AMDiS,which allows for adaptive mesh refinement, multi-level solvers and parallelization to thousands of processors. Using the DCA method (see Sect. 6), when analyzing problems with periodic motions, the needed calculation effort can be further reduced significantly. In case of a cyclic layout of the production process, such periodicities are often found.

One main goal of the CRC/TR 96 is a control-integrated error correction of the machine tool during the process. Due to this and to enable CPU-intensive tasks like optimization, the essential demand to the model is fast or even real-time computability of the problem. To comply with this, the MOR approach (see Sect. 5) deals with simulation models of reduced order. The proposed methods allow us to extract the essential information of the large and highly resolved models in terms of a reduced order model. Based on these compressed models, real-time computations and an implementation of the simulation methods on, for example machine controllers, become realizable. Thus, further important tasks within the development of applied MOR-methods in the CRC/TR 96 are to increase the reliability of these methods by ongoing improvements and to sensitize the end user to this problem accordingly.

Acknowledgments The authors thank the German Research Foundation for funding this work within the CRC/TR 96 and ZIH for the provided computing resources. We further thank Alexander Galant for providing the example used here.

References

1. Antoulas AC (2005) Approximation of large-scale dynamical systems. SIAM Publications, Philadelphia

2. Baur U, Beattie CA, Benner P, Gugercin S (2011) Interpolatory projection methods for parameterized model reduction. SIAM J Sci Comput 33(5):2489–2518
3. Calvo M, Chartier P, Murua A, Sanz-Serna J (2011) Numerical stroboscopic averaging for odes and daes. Appl Numer Math 61(10):1077–1095. doi:10.1016/j.apnum.2011.06.007
4. Weinan E, Engquist B (2003) The heterognous multiscale methods. Commun Math Sci 1(1):87–132
5. Freitas F, Rommes J, Martins N (2008) Gramian-based reduction method applied to large sparse power system descriptor models. IEEE Trans Power Syst 23(3):1258–1270
6. Großmann K, Städel C, Galant A, Mühl A (2012) Werkzeugmaschinen-Berechnung von Temperaturfeldern an Werkzeugmaschinen. Zeitschrift fur Wirtschaftlichen Fabrikbetrieb 107(6):452–456
7. Gerisch A, Naumann A, Wensch J (2015) Defect corrected averaging for highly oscillatory problems. Appl Math Comput 261(0):90–103
8. Gugercin S, Antoulas AC, Beattie C (2008) $\mathcal{H}_2$ model reduction for large-scale dynamical systems. SIAM J Matrix Anal Appl 30(2):609–638
9. Haasdonk B, Ohlberger M (2009) Efficient reduced models for parametrized dynamical systems by offline/online decomposition. In: Proceedings of MATHMOD 2009, 6th Vienna international conference on mathematical modelling
10. Hüeber S, Wohlmuth B (2009) Thermo-mechanical contact problems on non-matching meshes. Comput Methods Appl Mech Eng 198:1338–1350
11. Jungnickel G (2010) Simulation des thermischen Verhaltens von Werkzeugmaschinen/Modellierung und Parametrierung. Inst. für Werkzeugmaschinen und Steuerungstechnik, Lehrstuhl für Werkzeugmaschinen, Inst. für Werkzeugmaschinen und Steuerungstechnik, Lehrstuhl für Werkzeugmaschinen, Dresden
12. Lang N, Saak J, Benner P (2014) Model order reduction for systems with moving loads. at-Automatisierungstechnik 62(7):512–522
13. Nestmann S (2006) Mittel und Methoden zur Verbesserung des thermischen Verhaltens von Werkzeugmaschinen. In: Reinhart G, Zäh M (eds) IWB Seminarberichte, vol 83. Herbert Utz Verlag
14. Partzsch M, Beitelschmidt M (2015) Simulation of pose- and process-dependent machine tool models. In: Großmann K (ed) Thermo-energetic design of machine tools, chap. 6, pp 61–68. Springer International Publishing, Switzerland. doi:10.1007/978-3-319-12625-8_6
15. Saad Y, Schultz MH (1986) Gmres: a generalized minimal residual algorithm for solving nonsymmetric linear systems. SIAM J Sci Stat Comput 7(3):856–869
16. Strehmel K, Weiner R, Podhaisky H (2012) Numerik gewöhnlicher Differentialgleichungen/nichtsteife, steife und differential-algebraische Gleichungen, 2., überarb. und erw. aufl. edn. Springer Spektrum, Springer Spektrum
17. Verwer J, Spee E, Blom J, Hundsdorfer W (1999) A second-order Rosenbrock method applied to photochemical dispersion problems. SIAM J Sci Comput 20(4):1456–1480. doi:10.1137/S1064827597326651
18. Witkowski T, Ling S, Praetorius S, Voigt A (2015) Software concepts and numerical algorithms for a scalable adaptive parallel finite element method. Advances in computational mathematics, pp 1–33. doi:10.1007/s10444-015-9405-4